

# Multiwaveguide implantable probe for light delivery to sets of distributed brain targets

Anthony N. Zorzos,<sup>1,2,3</sup> Edward S. Boyden,<sup>1,2,\*</sup> and Clifton G. Fonstad<sup>2,3</sup>

<sup>1</sup>MIT Media Lab Synthetic Neurobiology Group, Departments of Brain and Cognitive Sciences and Biological Engineering, and MIT McGovern Institute, 77 Massachusetts Avenue, Cambridge, Massachusetts 02139, USA

<sup>2</sup>MIT Microsystems Technology Laboratory, 77 Massachusetts Avenue, Cambridge, Massachusetts 02139, USA

<sup>3</sup>MIT Department of Electrical Engineering and Computer Science, Massachusetts Institute of Technology, 77 Massachusetts Avenue, Cambridge, Massachusetts 02139, USA

\*Corresponding author: esb@media.mit.edu

Received September 9, 2010; accepted October 20, 2010;  
posted November 9, 2010 (Doc. ID 134680); published December 8, 2010

Optical fibers are commonly inserted into living tissues such as the brain in order to deliver light to deep targets for neuroscientific and neuroengineering applications such as optogenetics, in which light is used to activate or silence neurons expressing specific photosensitive proteins. However, an optical fiber is limited to delivering light to a single target within the three-dimensional structure of the brain. We here demonstrate a multiwaveguide probe capable of independently delivering light to multiple targets along the probe axis, thus enabling versatile optical control of sets of distributed brain targets. The 1.45-cm-long probe is microfabricated in the form of a 360- $\mu\text{m}$ -wide array of 12 parallel silicon oxynitride (SiON) multimode waveguides clad with SiO<sub>2</sub> and coated with aluminum; probes of custom dimensions are easily created as well. The waveguide array accepts light from a set of sources at the input end and guides the light down each waveguide to an aluminum corner mirror that efficiently deflects light away from the probe axis. Light losses at each stage are small (input coupling loss,  $0.4 \pm 0.3$  dB; bend loss, negligible; propagation loss,  $3.1 \pm 1$  dB/cm using the outscattering method and  $3.2 \pm 0.4$  dB/cm using the cutback method; corner mirror loss,  $1.5 \pm 0.4$  dB); a waveguide coupled, for example, to a 5 mW source will deliver over 1.5 mW to a target at a depth of 1 cm. © 2010 Optical Society of America

OCIS codes: 170.0170, 130.2755, 130.3120, 130.3990, 230.3990, 230.7370.

The ability to deliver light into the brain for the purposes of controlling neural activity and other biological processes has opened up new frontiers in both basic neuroscience and neuroengineering. One arena of great activity is in the use of microbial opsins such as channelrhodopsin-2 [1], *N. pharaonis* halorhodopsin [2,3], and archaerhodopsin-3 [4] to make neurons activatable or silencing by different colors of light, thus enabling assessment of the causal contribution of specific neurons, brain regions, or neural pathways to normal and abnormal behaviors and neural computations. To date, numerous *in vivo* studies have used optical fibers to deliver blue, yellow, or green laser light into brain targets in which certain neurons are expressing these opsins, but optical fibers can target just a single region. An implantable probe capable of delivering light to multiple points along the probe axis would enable more versatile optical control, opening up the ability to deliver patterned light to manipulate neural activity in different parts of a brain circuit in a systematic fashion, while greatly reducing surgical complexity and brain damage. We here describe the design and fabrication of a linear probe capable of multipoint independent light delivery and find that this design enables the efficient delivery of light to multiple targets along the probe axis, appropriate for delivering light to different lamina of the cortex, or to brain circuits of extended or complex shape, and potentially opening up the ability to screen for neural targets in a high-throughput fashion. Given the recent demonstration of precision cell type-specific optical control in the rhesus macaque cortex [5], such multiwaveguide probes may also enable a new kind of optical neural control prosthetic, opening up a new modality for neuromodulation treatment of brain disorders.

The probe design [Figs. 1(a) and 1(c)] comprises a parallel array of silicon oxynitride (SiON,  $n = 1.53$ ) rectangular waveguide cores (here, 20  $\mu\text{m}$  wide and 9  $\mu\text{m}$  thick), each coated with 3  $\mu\text{m}$  of SiO<sub>2</sub> cladding ( $n = 1.46$ ) and having a pitch of 30  $\mu\text{m}$ . SiON was chosen as the waveguide material because of its strength and well-characterized waveguiding properties [6–9], as well as its ability to have its index of refraction specified by tuning the SiO<sub>2</sub>:Si<sub>3</sub>N<sub>4</sub> ratio during plasma-enhanced chemical vapor deposition (PECVD) ( $n = 1.46$  for SiO<sub>2</sub>;  $n = 2.05$  for Si<sub>3</sub>N<sub>4</sub>). Our waveguides are large compared to most SiON waveguides [10,11] for this first demonstration, but the core width and pitch can easily be scaled down for closer waveguide packing. The demonstration device has a uniform thickness of 625  $\mu\text{m}$ , largely owing to the thickness of the supporting silicon; the probes can be made thinner (down to 50  $\mu\text{m}$  or less) with a backside deep reactive-ion etch step.

The waveguides each have an input end [Fig. 1(a), top] that can be coupled to a laser or other light source through appropriate optics (e.g., a fiber ribbon cable). Beyond the input segment, the waveguides converge into a thin probe shank via 750  $\mu\text{m}$  radius-of-curvature bends [Fig. 1(a), top inset]. The waveguides then run down the length of the probe until each reaches its desired independent depth [Fig. 1(a), bottom], at which point each waveguide terminates upon a straight-guide sidewall section coated with aluminum (Al), which acts as a corner mirror that reflects light 90° perpendicular to the probe axis [Fig. 1(a), bottom inset]. An abrupt turn minimizes probe width, and the Al coating augments the performance of the core-cladding index step [12,13].

In the present example probe, the waveguide width broadens to 60  $\mu\text{m}$  at the final terminus (i.e., the end

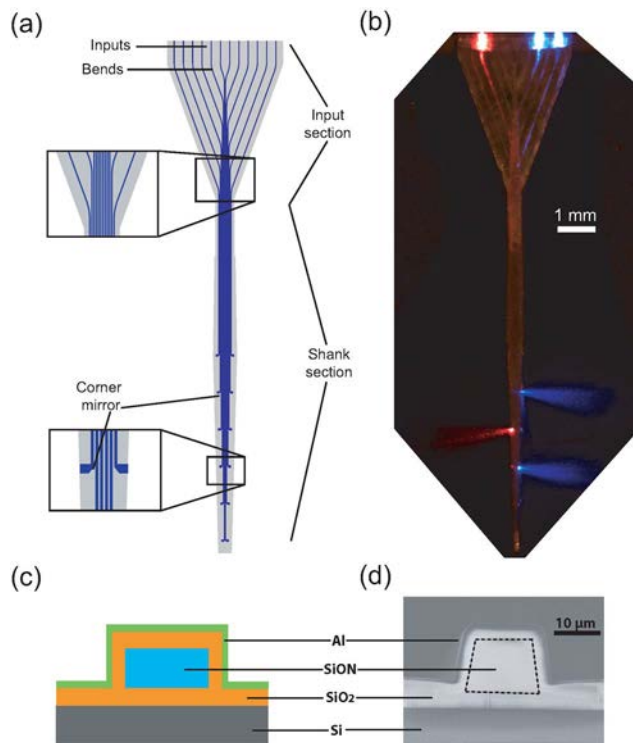


Fig. 1. (Color online) Design and fabrication of a multiwaveguide probe capable of independent light delivery to multiple targets along the probe axis. (a) Schematic of an example waveguide probe,  $360\ \mu\text{m}$  wide, and containing 12 waveguides, with inputs, bends, shanks, and corner mirrors labeled. (b) Photomicrograph of a waveguide probe fabricated according to the design in (a), with light coupled into 3 of the 12 waveguides and immersed in a scattering medium, showing emission of 473 nm and 632 nm light out three separate ports. (c) Cross section of a single waveguide, taken through the shank section of the probe. (d) SEM of a single waveguide, for the cross section shown in (c).

to be inserted in the brain) to spread light out; larger or smaller output apertures can be used as desired. The waveguide termini are spaced 1 mm along the probe shank, providing a dozen independently controllable outputs; this too is an easily customized property of the probe. The entire probe can be coated with a thin transparent biocompatible coating (e.g., oxide, Parylene, etc.) before insertion into the brain. An example probe fabricated with these geometries, and illuminated with three independent laser light sources, is shown in Fig. 1(b). The waveguide probe fabrication process utilizes standard microfabrication techniques. First, a  $3\ \mu\text{m}$  layer of  $\text{SiO}_2$  is PECVD deposited on a standard 6 in. Si wafer to form the lower cladding of the waveguides. A  $9\ \mu\text{m}$  SiON waveguide layer is then PECVD deposited on top of the  $\text{SiO}_2$  layer. A thick photoresist mask is next patterned, and the pattern transferred to the SiON using a plasma etch that terminates at the wafer surface to define the waveguides, followed by a double piranha ( $3:1$ ,  $\text{H}_2\text{SO}_4:\text{H}_2\text{O}_2$ ) clean. A second  $3\ \mu\text{m}$   $\text{SiO}_2$  cladding layer is deposited, followed by 300 nm of sputtered aluminum [final cross section shown in Fig. 1(c); scanning electron microscope (SEM) of cleaved probe at this stage shown in Fig. 1(d)]. The Al layer is removed from the probe side-walls at the input and output facets in a mask and wet

etch step. Finally the wafer is mounted via photoresist on a quartz handle wafer, followed by probe freeing from the silicon wafer by a Bosch process through-wafer etch and then finally dissolution of the photoresist mounting. The overall length of these initial probes is 1.45 cm from fiber input to probe tip (narrow probe shank portion, 1 cm long).

To characterize the probes, a multiguide probe is mounted on a stage, and a fiber ribbon cable containing 12 single-mode fibers ( $8\ \mu\text{m}$  diameter core,  $125\ \mu\text{m}$  diameter cladding; Timbercon, Inc.) is aligned to the 12 inputs. The other end of the fiber ribbon cable docks to a cassette that couples each fiber to a separate laser source; for Fig. 1(b), two 473 nm diode-pumped solid-state lasers (Optoengine, Inc.) and a conventional 632 nm He-Ne laser were used to demonstrate the probe's ability to deliver different colors of light to three targets along the probe axis. The light transmission properties of the probe were quantified by determining the loss in each part of the probe: loss at the coupling to the input, loss in propagation of light through the guide, and loss at the corner mirror. Two independent methods were used: an image-based out-scattering technique in which the light scattered out of the waveguide is measured [14,15] and a direct measurement cutback method in which the light that comes out of the probe after it is truncated to different lengths is measured [16,17].

The outscattering technique requires that the topside aluminum layer be chemically stripped, leaving optical access to the waveguides. While this method only measures relative loss, it has the advantage of allowing for examination of the heterogeneity of the light loss all along the probe. Scattered light intensity values were measured by imaging the probe topside on a complementary metal-oxide semiconductor camera while illuminating with the 473 nm laser (continuous power  $\sim 0.5\ \text{mW}$ ) and plotting these light intensity values against distance along each guide, from its input end to the  $90^\circ$  mirror, as shown for a representative guide in Fig. 2(a). The amount of light scattered out of any segment along the waveguide is a function of two parameters: the energy flux and local geometry. In this case, roughness at the core-cladding interface causes the scattering and is assumed to be constant along the length of the waveguide. This yields a constant proportionality between energy flux and scattered light intensity, and therefore propagation loss at a given point on the probe is reflected by the slope of the smoothed curve at that point. We performed measurements on 20 waveguides on two separate probes, and fit each image profile with a line (median  $R^2$  of the curve fits, 0.97; range, 0.92–0.99; curves fitted using least-squares regression); the average line is plotted in Fig. 2(a) and yields a slope of  $3.1 \pm 1\ \text{dB/cm}$  loss (mean  $\pm$  standard deviation,  $n = 20$ ). The linear shape of these profiles indicates that propagation loss is constant along the waveguide and that the smooth bends introduce negligible additional loss, as would be expected given the strong index step (in principle, smaller bend radii could therefore be used).

In the cutback method, probes were truncated to various lengths, and then the output of one waveguide on each probe was measured with a photodiode (Si, Thorlabs) when that waveguide's input was illuminated with

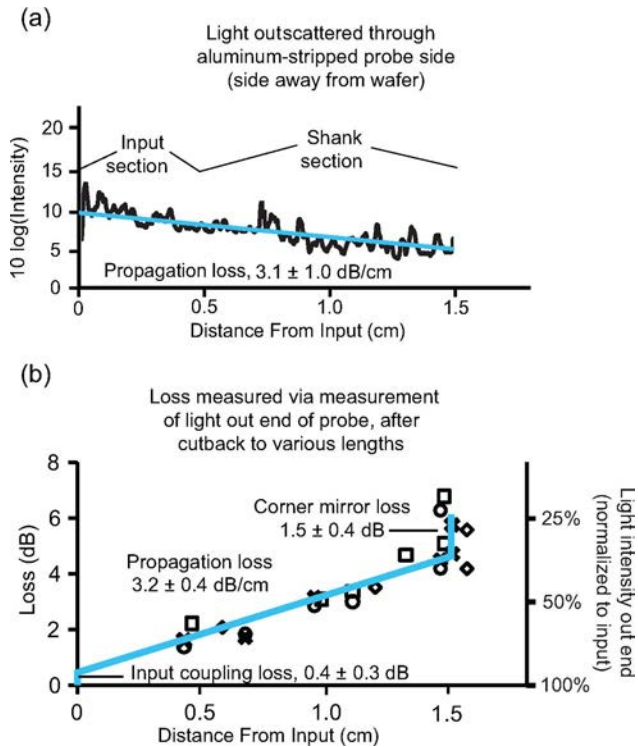


Fig. 2. (Color online) Characterization of multiwaveguide probe performance for a geometry appropriate for multisite neural target illumination. (a) Outscattering measured propagation loss for the input and shank sections of a representative guide. Shown is also the average linear fit for 20 waveguides (straight line). (b) Cutback characterization of loss at different points along four waveguides on different probes; different symbols indicate raw data taken from different waveguides. Shown is also the average multipart linear fit for four waveguides (straight lines).

a 473 nm laser [Fig. 2(b), different symbols indicate data from four different probes; blue line is the average of the four curve fits performed (median  $R^2$  of the curve fits, 0.98; range, 0.91–0.99; curves fitted using least-squares regression)]. While this analysis is limited to a few discrete points per probe, this method allows for absolute measurement of light loss at a given point in the waveguide. The propagation, corner mirror, and input coupling losses were, respectively,  $3.2 \pm 0.4$  dB/cm,  $1.5 \pm 0.4$  dB, and  $0.4 \pm 0.3$  dB ( $n = 4$ ). In the one probe parameter that can be measured with both methods, the propagation loss found was in excellent agreement (3.1 versus 3.2 dB/cm for the outscattering and cutback methods, respectively).

In terms of light delivery efficiency, the measurements demonstrate that these first multiwaveguide probes typically deliver 33% of the fiber input source optical power from the uppermost output port, which is 4.5 mm from the top of the probe shank, and 23% from the deepest output port, which is 9.5 mm deep. (The percent of light delivered from deeper ports is reduced due to the additional propagation loss.) These depths are comparable to the sizes of circuits in the mammalian brain, and this functionality is sufficient to engender exciting new experiments in neuroscience, opening up new frontiers in neural control. At the same time, there is clearly much room for improvement; it should be possible to reduce

propagation loss significantly, for example, by reducing sidewall roughness, and it will be easy to fabricate probes with higher guide packing densities and more illumination ports by reducing the widths of the guides and the spacing of their output ports.

We thank Jake Bernstein, Jorg Scholvin, and the MIT Microsystems Technology Laboratories for assistance and consultation on this project. C. G. F. and E. S. B. acknowledge support from the MIT McGovern Institute Neurotechnology Program, the Paul Allen Family Foundation, and National Institutes of Health (NIH). A. N. Z. acknowledges support from a National Science Foundation (NSF) graduate fellowship. E. S. B. additionally acknowledges funding by NSF, Department of Defense Congressionally Directed Medical Research Programs Post Traumatic Stress Disorder Program, National Alliance for Research on Schizophrenia and Depression, Alfred P. Sloan Foundation, Jerry and Marge Burnett, Society for Neuroscience Research Awards for Innovation in Neuroscience award, MIT Media Lab, Benesse Foundation, and Wallace H. Coulter Foundation.

## References

1. E. S. Boyden, F. Zhang, E. Bamberg, G. Nagel, and K. Deisseroth, *Nat. Neurosci.* **8**, 1263 (2005).
2. X. Han and E. S. Boyden, *PLoS ONE* **2**, e299 (2007).
3. F. Zhang, L. P. Wang, M. Brauner, J. F. Liewald, K. Kay, N. Watzke, P. G. Wood, E. Bamberg, G. Nagel, A. Gottschalk, and K. Deisseroth, *Nature* **446**, 633 (2007).
4. B. Y. Chow, X. Han, A. S. Dobry, X. Qian, A. S. Chuong, M. Li, M. A. Henninger, G. M. Belfort, Y. Lin, P. E. Monahan, and E. S. Boyden, *Nature* **463**, 98 (2010).
5. X. Han, X. Qian, J. G. Bernstein, H. H. Zhou, G. T. Franzesi, P. Stern, R. T. Bronson, A. M. Graybiel, R. Desimone, and E. S. Boyden, *Neuron* **62**, 191 (2009).
6. M. Hoffmann, P. Kopka, and E. Voges, *IEEE Photonics Technol. Lett.* **9**, 1238 (1997).
7. K. W. Renee, M. de Ridder, A. Driessen, P. V. Lambeck, and H. Albers, *IEEE J. Sel. Top. Quantum Electron.* **4**, 930 (1998).
8. K. Worhoff, A. Driessen, P. V. Lambeck, L. T. H. Hilderink, P. W. C. Linders, and T. J. A. Popma, *Sens. Actuators A* **74**, 9 (1999).
9. K. Worhoff, P. V. Lambek, and A. Driessen, *J. Lightwave Technol.* **17**, 1401 (1999).
10. T. Barwicz and H. A. Haus, *J. Lightwave Technol.* **23**, 2719 (2005).
11. C. G. Poulton, C. Koos, M. Fujii, A. Pfrang, T. Schimmel, J. Leuthold, and W. Freude, *IEEE J. Sel. Top. Quantum Electron.* **12**, 1306 (2006).
12. S. Lardenois, D. Pascal, L. Vivien, E. Cassan, S. Laval, R. Orobtcchouk, M. Heitzmann, N. Bouzaida, and L. Mollard, *Opt Lett.* **28**, 1150 (2003).
13. Y. Qian, S. Kim, J. Song, and G. P. Nordin, *Opt. Express* **14**, 6020 (2006).
14. Y. Okamura, S. Yoshinaka, and S. Yamamoto, *Appl. Opt.* **22**, 3892 (1983).
15. V. Subramaniam, G. N. DeBrabander, D. H. Naghski, and J. T. Boyd, *J. Lightwave Technol.* **15**, 990 (1997).
16. G. T. Reed, in *IEEE Colloquium on Measurements on Optical Devices* (IEEE, 1992), pp. 2/1–2/7.
17. A. L. Zhang and K. T. Chan, in *Proceedings of the Sixth Chinese Optoelectronics Symposium* (IEEE, 2003), Vols. 124–127, p. 296.